Routes to Chaos in the Peroxidase–Oxidase Reaction. 2. The Fat Torus Scenario

ARTICLE *in* THE JOURNAL OF PHYSICAL CHEMISTRY B · JULY 1998

Impact Factor: 3.3 · DOI: 10.1021/jp9720496

Routes to Chaos in the Peroxidase−Oxidase Reaction. 2. The Fat Torus Scenario

Tatiana V. Bronnikova[†] and William M. Schaffer*

Department of Ecology and Evolutionary Biology University of Arizona Tucson, Arizona 85721

Marcus J. B. Hauser and Lars F. Olsen

Physical Biochemistry Group, Institute of Biochemistry, Odense University, Forskerparken 10, DK-5230 Odense M, Denmark

Received: June 24, 1997; In Final Form: October 20, 1997[⊗]

Experimental studies [Hauser, M. J. B.; Olsen, L. F. *J. Chem. Soc., Faraday Trans.* **1996**, *92*, 2857−2863] of the peroxidase−oxidase (PO) reaction at pH values in excess of 5.4 suggest the existence of narrow regions of complex dynamics between adjacent mixed-mode oscillations (MMOs) that occur in period-adding sequences. Previously [Hauser, M. J. B.; Olsen, L. F.; Bronnikova, T. V.; Schaffer, W. M. *J. Phys. Chem. B* **1997**, *101*, 5075−5083], it was argued that both the period-adding sequences and the transitional regions between neighboring MMOs are predictable by a detailed model of the reaction called BFSO [Bronnikova, T. V.; Fed'kina, V. R.; Schaffer, W. M.; Olsen, L. F. *J. Phys. Chem.* **1995**, *99*, 9309−9312]. In the present paper, we study the transitional regions via computer simulation. Our investigations indicate that the motion therein may be periodic, quasiperiodic, or chaotic. In greater detail, we observe a quasiperiodic route to chaos whereby period-doubled cycles give rise to doubled tori that, in turn, undergo homoclinic bifurcations to chaos. Because the latter transitions are a consequence of progressive fattening of the tori, we propose calling this scenario the "fat torus" route to chaos, and the homoclinic bifurcations "fat torus" bifurcations (FTBs). The numerical results are qualitatively consistent with the experimental findings reported to date. FTBs and the resultant period-doubled, fractal tori may provide a criterion for discriminating among alternative models of the PO reaction.

I. Introduction

In recent years, the peroxidase-catalyzed oxidation of NADH by molecular oxygen has become a model system for the study of complex biochemical dynamics. This reaction is commonly referred to as the peroxidase−oxidase (PO) reaction, even though, strictly speaking, the term applies to any reaction in which a hydrogen donor is oxidized in the presence of peroxidase enzyme with oxygen serving as the oxidant. Terminology aside, the overall stoichiometry of the reaction is

$$2\mathrm{NADH} + \mathrm{O_2} + 2\mathrm{H^+} \rightarrow 2\mathrm{NAD^+} + 2\mathrm{H_2O} \qquad (1)$$

In previous submissions,[1−3] it was reported that the reaction's *qualitative* response to increasing rates of NADH input is pH-dependent. For pH values ranging from 5.2 to 5.3, increasing NADH input induces period-doubling bifurcations to chaos. Conversely, for pH = 5.5−6.3, the transition to chaos is preceded by mixed-mode oscillations (MMOs) arranged in a period-adding sequence. Elsewhere,[1] we have argued that, at least to first order, increasing pH can be modeled by reducing the rate constant, k_9, in

$$2\mathrm{NAD^\bullet} \xrightarrow{k_9} (\mathrm{NAD})_2 \qquad (\mathrm{R9})$$

Under this assumption, the experimental results are broadly reproducible by a detailed model of the reaction called BFSO.[4] This model implements the mechanism displayed in Table 1 as a system of 10 coupled differential equations. BFSO is similar to the Urbanalator[5] from which it differs by the *inclusion* of reactions that entail the conversion of ferric peroxidase ($\mathrm{Per^{3+}}$) to ferrous peroxidase ($\mathrm{Per^{2+}}$) and $\mathrm{Per^{2+}}$ to oxyferrous peroxidase which is also called compound III (coIII). Both models, along with other related schemes[6−17] derive from the work of Yokota and Yamazaki.[18]

The rationale for using k_9 as a proxy parameter for pH is discussed in ref 1. Here it is argued that decreases in pH will lead to reductions in the net negative charge on $\mathrm{NAD^\bullet}$ and hence to increasing values of k_9 due to reduced Coulombic repulsion between $\mathrm{NAD^\bullet}$ molecules. More precisely, for pH values between 2 and 7, NAD radicals carry a net negative charge and are subject to pH-dependent protonation−deprotonation as reflected by the pK_a values of $\mathrm{NAD^+}$ (3.35) and NADH (3.65).[1] Increasing pH will make these radicals more negative, thereby reducing the rate of dimerization, $2\mathrm{NAD^\bullet} \rightarrow (\mathrm{NAD})_2$ (R9) and, hence, the magnitude of the rate constant, k_9. As to the scaling of k_9 with pH, we associate k_9 values for which a particular MMO is the most complex induced by the model with a corresponding range of pH values for which the *same* MMO is the most complex observed experimentally. As documented in ref 1, this approach, while frankly pragmatic,

[†] Permanent address: Institute of Theoretical & Experimental Biophysics, Russian Academy of Sciences, Pushchino 142292, Moscow Region, Russia.

* To whom correspondence should be sent. FAX: 520-621-9190. Email: schaffer@ccit.arizona.edu.

[⊗] Abstract published in *Advance ACS Abstracts,* December 15, 1997.

S1089-5647(97)02049-X CCC: $15.00
Published on Web 01/15/1998

TABLE 1: Elementary Steps in PO Reaction

reaction	R_l	constant
1. $NADH + O_2 + H^+ \xrightarrow{k_1} NAD^+ + H_2O_2$	$k_1[NADH][O_2]$	$k_1 = 3\ M^{-1}\ s^{-1}$
2. $H_2O_2 + Per^{3+} \xrightarrow{k_2} coI$	$k_2[H_2O_2][Per^{3+}]$	$k_2 = 1.8 \times 10^7\ M^{-1}\ s^{-1}$
3. $coI + NADH \xrightarrow{k_3} coII + NAD^•$	$k_3[coI][NADH]$	$k_3 = 4.0 \times 10^4\ M^{-1}\ s^{-1}$
4. $coII + NADH \xrightarrow{k_4} Per^{3+} + NAD^•$	$k_4[coII][NADH]$	$k_4 = 2.6 \times 10^4\ M^{-1}\ s^{-1}$
5. $NAD^• + O_2 \xrightarrow{k_5} NAD^+ + O_2^-$	$k_5[NAD^•][O_2]$	$k_5 = 2.0 \times 10^7\ M^{-1}\ s^{-1}$
6. $O_2^- + Per^{3+} \xrightarrow{k_6} coIII$	$k_6[O_2^-][Per^{3+}]$	$k_6 = 1.7 \times 10^7\ M^{-1}\ s^{-1}$
7. $2O_2^- + 2H^+ \xrightarrow{k_7} H_2O_2 + O_2$	$k_7[O_2^-]^2$	$k_7 = 2.0 \times 10^7\ M^{-1}\ s^{-1}$
8. $coIII + NAD^• \xrightarrow{k_8} coI + NAD^+$	$k_8[coIII][NAD^•]$	$k_8 = 9.0 \times 10^7\ M^{-1}\ s^{-1}$
9. $2NAD^• \xrightarrow{k_9} (NAD)_2$	$k_9[NAD^•]^2$	$k_9 =$ variable
10. $Per^{3+} + NAD^• \xrightarrow{k_{10}} Per^{2+} + NAD^+$	$k_{10}[Per^{3+}][NAD^•]$	$k_{10} = 1.8 \times 10^6\ M^{-1}\ s^{-1}$
11. $Per^{2+} + O_2 \xrightarrow{k_{11}} coIII$	$k_{11}[Per^{2+}][O_2]$	$k_{11} = 1.0 \times 10^5\ M^{-1}\ s^{-1}$
12. $NADH(stock) \xrightarrow{k_{12}} NADH(liquid)$	$k_{12}[NADH]_{st} =$ variable	
13. $O_2(gas) \underset{k_{-13}}{\overset{k_{13}}{\rightleftharpoons}} O_2(liquid)$	$k_{13}[O_2]_{eq} = 7.2 \times 10^{-8}\ M\ s^{-1}$ $k_{-13}[O_2]$	$k_{-13} = 6.0 \times 10^{-3}\ s^{-1}$

nevertheless allows for successful modeling of the experimental phenomenology.

An interesting feature of the experimental results is the presence of regions of transitional dynamics between adjacent MMOs for pH > 5.4. Within these regions, one observes period-doubled states, for example $(1^0)^2$ cycles between the 1^0 and 1^1 states, i.e., in the 1^0-1^1 region, as well as periodic and/or apparently chaotic mixtures of the neighboring MMOs. In the present paper, we suggest that these findings are consistent with the BFSO scheme as implemented in ref 1. We also consider the evolution of the transitional regions in response to changing values of k_9. In this regard, we show that BFSO predicts a quasiperiodic route to chaos involving homoclinic bifurcations of period-doubled tori. The present study thus makes contact with our previous finding[20] of "secondary" quasiperiodicity, i.e., motion on $2n$ tori, in the BFSO model, thereby underscoring the potential importance of quasiperiodic flow in eq 1.

Although our concern here is the PO reaction's response to variations in NADH input, we note that homoclinic transitions from secondary quasiperiodicity to chaos are also predicted to occur in response to varying the equilibrium concentration of oxygen, $[O_2]_{eq}$, in the gas phase. Such transitions may thus be observable under a variety of experimental conditions.

II. Experimentally Observed Transitional States

Figure 1 summarizes the experimental situation for pH 6.3. (For methodological details, see ref 1.) With increasing NADH input, the primary sequence of MMOs is 1^0, 1^1, 1^2, 1^3, and 1^4, where L^S indicates a cycle consisting of L large-amplitude excursions followed by S small-amplitude oscillations per repeating unit. A chaotic region (C), follows the 1^4 cycle and is, itself, succeeded by small amplitude, period-two oscillations, denoted 0^2. The latter undergo reverse bifurcation and finally yield to a steady state (ss).

Additional states between the primary MMOs were also observed. Of these, four were stabilized experimentally (Figure 1):

1. In the 1^0-1^1 region: Period-doubled 1^0 cycles, i.e., $(1^0)^2$ oscillations.

2. In the 1^1-1^2 region: (a) Period-doubled 1^1 cycles, i.e., $(1^1)^2$ oscillations, and (b) Chaotic mixtures of 1^1 and 1^2 cycles.

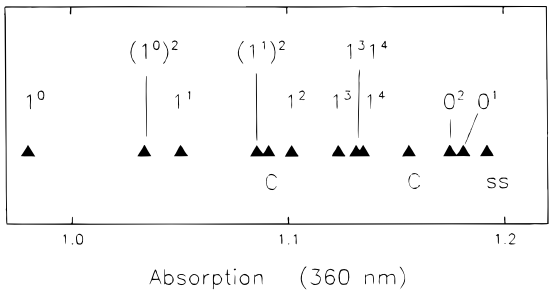

Figure 1. Dynamical states observed experimentally at pH 6.3. Absorption at 360 nm monitors averaged concentration of NADH. MMOs labeled according to L^S notation, i.e., L large-amplitude excursions followed by S small-amplitude oscillations. $(L^S)^2$ indicates a period-doubled state, and L^SL^T, a concatenation of alternating cycles. C denotes chaos; 0^i, small amplitude cycles; and ss, the final steady state. Reproduced from ref 1.

TABLE 2: Differential Equations

$d[NADH]/dt$	=	$-R_1 - R_3 - R_4 + R_{12}$
$d[O_2]/dt$	=	$-R_1 - R_5 + R_7 + R_{13} - k_{-13}[O_2] - R_{11}$
$d[NAD^•]/dt$	=	$R_3 + R_4 - R_5 - R_8 - 2R_9 - R_{10}$
$d[Per^{3+}]/dt$	=	$-R_2 + R_4 - R_6 - R_{10}$
$d[coI]/dt$	=	$R_2 - R_3 + R_8$
$d[coII]/dt$	=	$R_3 - R_4$
$d[coIII]/dt$	=	$R_6 - R_8 + R_{11}$
$d[H_2O_2]/dt$	=	$R_1 - R_2 + R_7$
$d[O_2^-]/dt$	=	R_5 - $R_6 - 2R_7$
$d[Per^{2+}]/dt$	=	$R_{10} - R_{11}$

TABLE 3: Initial Conditions for Simulations (in μM)

$[NADH]_0 = 0.0$	$[O_2]_0 = 12.0$	$[NAD^•]_0 = 0.0$
$[Per^{3+}]_0 = 1.5$	$[coI]_0 = 0.0$	$[coII]_0 = 0.0$
$[coIII]_0 = 0.0$	$[H_2O_2]_0 = 0.0$	$[O_2^-]_0 = 0.0$
$[Per^{2+}]_0 = 0.0$		

3. In the 1^3-1^4 region: Alternating 1^3 and 1^4 cycles, i.e., (1^31^4) oscillations.

III. Simulations

The BFSO reaction scheme (Table 1) was implemented as shown in Table 2. Initial conditions for the bifurcation diagrams (Figures 3, 7a, and 9a) are given in Table 3. Initial conditions for the remaining figures correspond to the final values of the state variables generated by the bifurcation program for the parameter values in question.

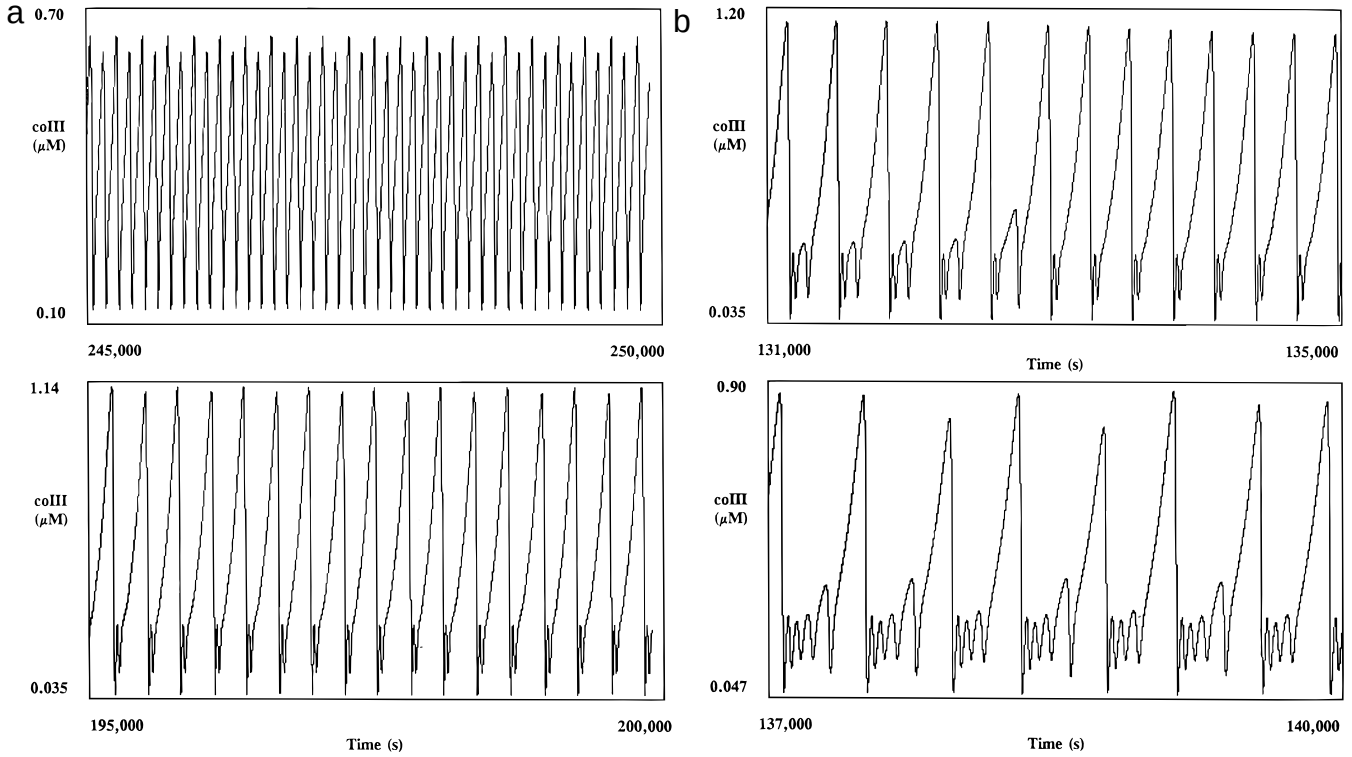

Figure 2. Simulated transitional time series. (a) Period-doubled oscillations in the 1^0-1^1 and 1^1-1^2 regions. Top: $(1^0)^2$ cycle. $k_9 = 1.1 \times 10^8$ M^{-1} s^{-1}. NADH input $= 0.12250 \times 10^{-6}$ M s^{-1}. Bottom: $(1^1)^2$ cycle. $k_9 = 0.40 \times 10^8$ M^{-1} s^{-1}. NADH input $= 0.10885 \times 10^{-6}$ M s^{-1}. (b) Complex dynamics in the 1^1-1^2 and 1^3-1^4 regions. $k_9 = 0.40 \times 10^8$ M^{-1} s^{-1}. Top: Chaos in the 1^1-1^2 region. NADH input $= 0.1100 \times 10^{-6}$ M s^{-1}. Bottom: A $1^3 1^4$ transient. NADH input $= 0.124\,65 \times 10^{-6}$ M s^{-1}.

As discussed in our previous publication, the experimental results reported in ref 1 are reproducible by BFSO in the sense that reducing k_9 (whereby we simulate increasing pH) induces a transition from period-doubling to period-adding. That is, both the primary periodic states and the sequence in which they occur are replicated by the model. On the other hand, if one restricts one's attention to the *experimental* range of NADH flow rates, not all of the states observed in the lab for single pH values are inducible by the model. Consider, for example, $k_9 = 4.0 \times 10^7$ M^{-1} s^{-1} which, by the argument of ref 1, mimics pH $=$ 6.3. For NADH input rates on the interval, [1×10^{-7} M s^{-1}, 1.3×10^{-7} M s^{-1}], the MMO of lowest period induced by the model is the 1^1 cycle, i.e., the 1^0 state is missing. We emphasize that this state *is* inducible by the model, but only at NADH input rates, e.g., $k_{12}[\mathrm{NADH}]_0 = 5.9 \times 10^{-8}$ M s^{-1}, well below the experimental minimum. To study the 1^0-1^1 region, we accordingly chose $k_9 = 1.1 \times 10^8$ M^{-1} s^{-1}. With this adjustment, period-doubled 1^0 and 1^1 states (Figure 2a), as well as chaotic mixtures of 1^S and 1^{S+1} cycles (Figure 2b, top) are reproducible by BFSO. Alternating 1^3 and 1^4 oscillations in the 1^3-1^4 region, were also observed (Figure 2b, bottom), but only as short runs. For this region, the model induces more complex periodic states, e.g., $(1^3)^2 1^4$ and $(1^3)^2(1^4)^2$ cycles, as well as apparently chaotic motions consisting principally of 1^3 and 1^4 cycles.

IV. Evolution of Transitional Regions in Response to Changing Values of k_9

Unlike the goddess Athena, who sprang complete in her development from the brow of Zeus, the transitional regions in BFSO do not arise fully formed. Instead, one observes a well-defined progression from period-doubled cycles to secondary quasiperiodicity to chaos on period-doubled fractal tori. So far as we are aware, this route to chaos has not been previously described. Accordingly, we propose the name "fat torus scenario". Our choice of terminology reflects the fact that chaos in the transitional regions results from the progressive "fattening" of period-doubled tori, a process that seems to culminate in a homoclinic event involving the stable and unstable manifolds of a nonstable periodic orbit. For the latter transition, we propose the term "fat torus bifurcation" (FTB).

The 1^0-1^1 Region. The fat torus scenario is most readily understood by considering the evolution of the 1^0-1^1 region in response to decreasing values of the rate constant, k_9. As argued in ref 1, this mimics the effect of progressive reductions in pH. For pedagogic purposes, we begin with $k_9 = 1.20 \times 10^8$ M^{-1} s^{-1}, even though the corresponding pH ≈ 4.8 is below the value at which NADH dissociation becomes significant. We then consider successively smaller values of k_9, concluding with $k_9 = 0.60 \times 10^8$ M^{-1} s^{-1} which, by the argument of ref 1, corresponds to pH ≈ 5.7. Our analysis is summarized by way of bifurcation diagrams (Figure 3), asymptotic trajectories projected to three dimensions, [O_2], [NAD$^\bullet$], and [NADH] (Figure 4a,c,e), and Poincaré sections (Figure 4b,d,f). We also display next amplitude maps (Figure 5) for which we were able to accurately accumulate a large number of points. For generic systems, the latter are topologically equivalent to the Poincaré sections.

With reference to the aforementioned illustrations, we identify the following stages in the region's evolution:

1. Period-Bubbling. $k_9 = 1.20 \times 10^8$ M^{-1} s^{-1}. Here the 1^0 (period-1) cycle undergoes conventional period-doubling and then remerges (Figure 3a). The failure of period-doubling cascades to accumulate, and their subsequent remerging is sometimes referred to as "period bubbling".[19]

2. Secondary Quasiperiodicity. $k_9 = 1.1 \times 10^8$ M^{-1} s^{-1}. The interval corresponding to period-2 dynamics is interrupted (Figure 3b) by a region of quasiperiodic behavior on a double

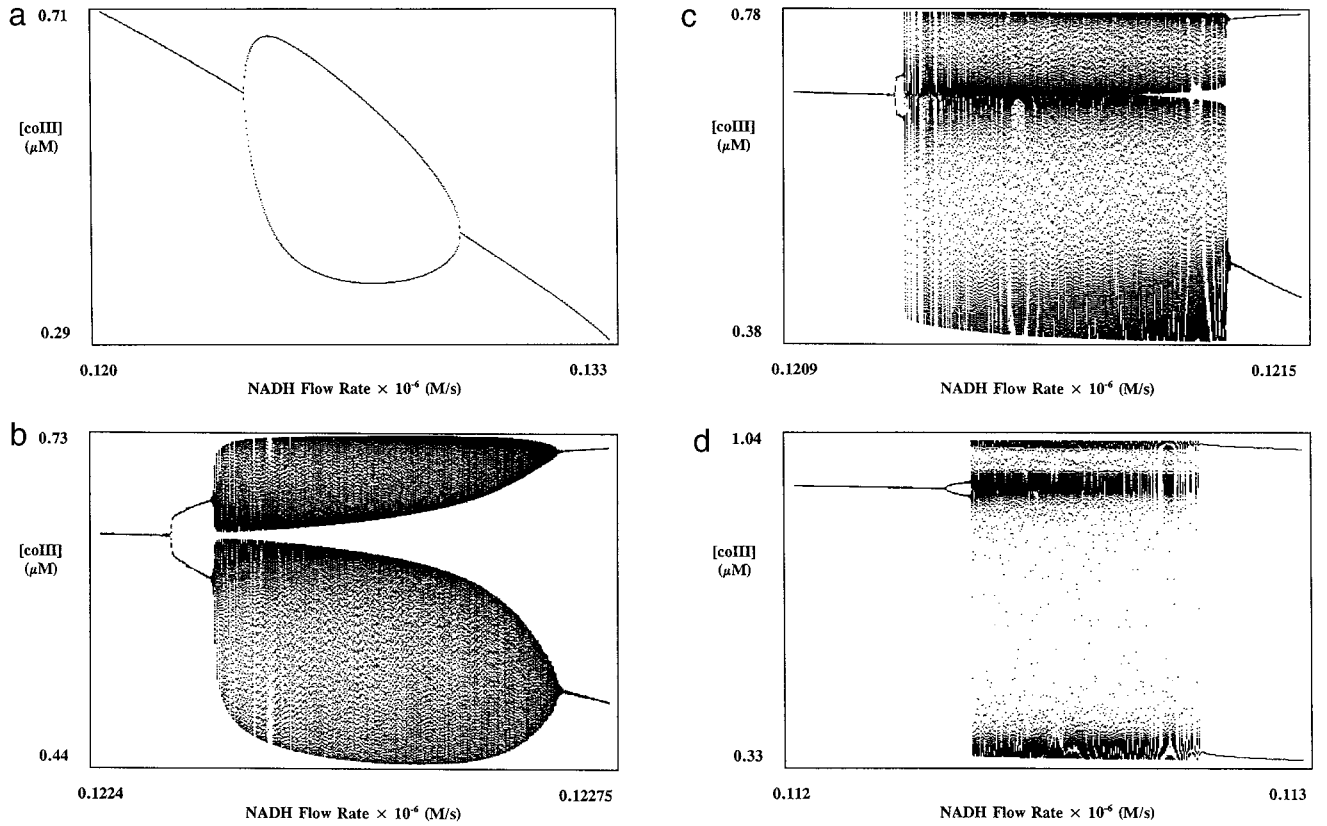

Figure 3. Bifurcation diagrams detailing the evolution of the 1^0-1^1 transitional region in response to decreasing values of the rate constant, k_9. (a) $k_9 = 1.2 \times 10^8$ M^{-1} s^{-1}. The period-1 cycle undergoes doubling and then remerges. (b) $k_9 = 1.1 \times 10^8$ M^{-1} s^{-1}. The twice-periodic regime is interrupted by quasiperiodic flow on a doubled torus. (c) $k_9 = 1.0 \times 10^8$ M^{-1} s^{-1}. The two pieces of the double torus overlap in projection. The actual tangency occurs at a somewhat lower k_9 value. (d) $k_9 = 0.7 \times 10^8$ M^{-1} s^{-1}. A narrow region of $(1^0)^2$ dynamics is succeeded by chaos on a fractal double torus.

torus (Figure 4a). The toroidal nature of the flow is confirmed by the Poincaré section (Figure 4b) which consists of two invariant loops. In this case, increasing the rate of NADH input induces an apparently smooth transition to "secondary quasiperiodicity"[20] via what one imagines to be a supercritical, secondary Hopf bifurcation. Correspondingly, the transition out of quasiperiodic dynamics, i.e., restoration of the period-2 cycle, also appears supercritical.

3. Approach to Tangency. $k_9 = 1.0 \times 10^8$ M^{-1} s^{-1}. As one further reduces k_9 (Figure 3c), the torus "fattens." This results in the doubled tubes approaching each other medially as shown in Figures 4c and 4d. The approach to tangency is most readily seen in the Poincaré section.

4. Homoclinic Bifurcation. $k_9 = 0.7 \times 10^8$ M^{-1} s^{-1}. Further reductions in k_9 (Figure 3d) result first in tangency and then in expansion of the zone of apparent contact between the two parts of the double torus (Figure 4e,f). As a result, the two halves of the Poincaré section appear to be joined Siamese-twin style at the midline. In fact, the "line" of contact turns out to consist of an apparently infinite number of layers as shown in Figure 5a. Here, we display a magnification of the next amplitude map computed by plotting successive maxima in coIII.

Returning to the bifurcation diagram (Figure 3d), we also note that as k_9 is reduced, the range of parameter values (NADH input) corresponding to complex dynamics expands both left and right until the onset and cessation of this regime are essentially coincident with the secondary Hopf bifurcations noted above.

5. Homoclinic Tangle. $k_9 = 0.6 \times 10^8$ M^{-1} s^{-1}. As we continue to reduce k_9, additional structure in the region of "contact" becomes apparent (Figure 5b). In particular, one sees the familiar "lobes" of a homoclinic tangle.[21] Moreover, the lobes become longer and thinner and apparently more tightly packed as one moves along the region of tangency in the direction indicated by the arrows.

In sum, we propose that progressive "fattening" of a 2-torus results in a homoclinic bifurcation (FTB) involving the stable and unstable manifolds of the period-1 saddle cycle, the approximate location of which is indicated by a + in Figure 5a,b. The approach to homoclinicity is depicted in Figure 6. Here, asymptotic motions in the phase space are displayed schematically as a series of Poincaré sections. Figure 6a shows the situation (high values of k_9) prior to period-doubling. Here, we see a simple periodic orbit in section, i.e., a fixed point, which is stable in all directions as indicated by the arrows that represent the eigenvectors (and their continuations) of the Poincaré map. Figure 6b depicts the situation (somewhat lower k_9) *after* period-doubling. The original cycle is now a saddle with stable and unstable manifolds. The two new fixed points of the map correspond to the points where the twice periodic orbit produced by the doubling intersects the section. Since the period-doubled orbit is stable, all initial conditions, save those precisely on the period-1 orbit and its stable manifold, induce trajectories asymptotic to the period-2 cycle. In Figure 6c (still lower values of k_9), the period-2 cycle is destabilized via a (secondary, supercritical) Hopf bifurcation. Iterates of the Poincaré map now trace out two invariant loops that correspond to a double torus in section. With further reductions in k_9, the double torus fattens so that its inner surfaces approach each other and the stable manifold of the period-1 cycle that lies between them.

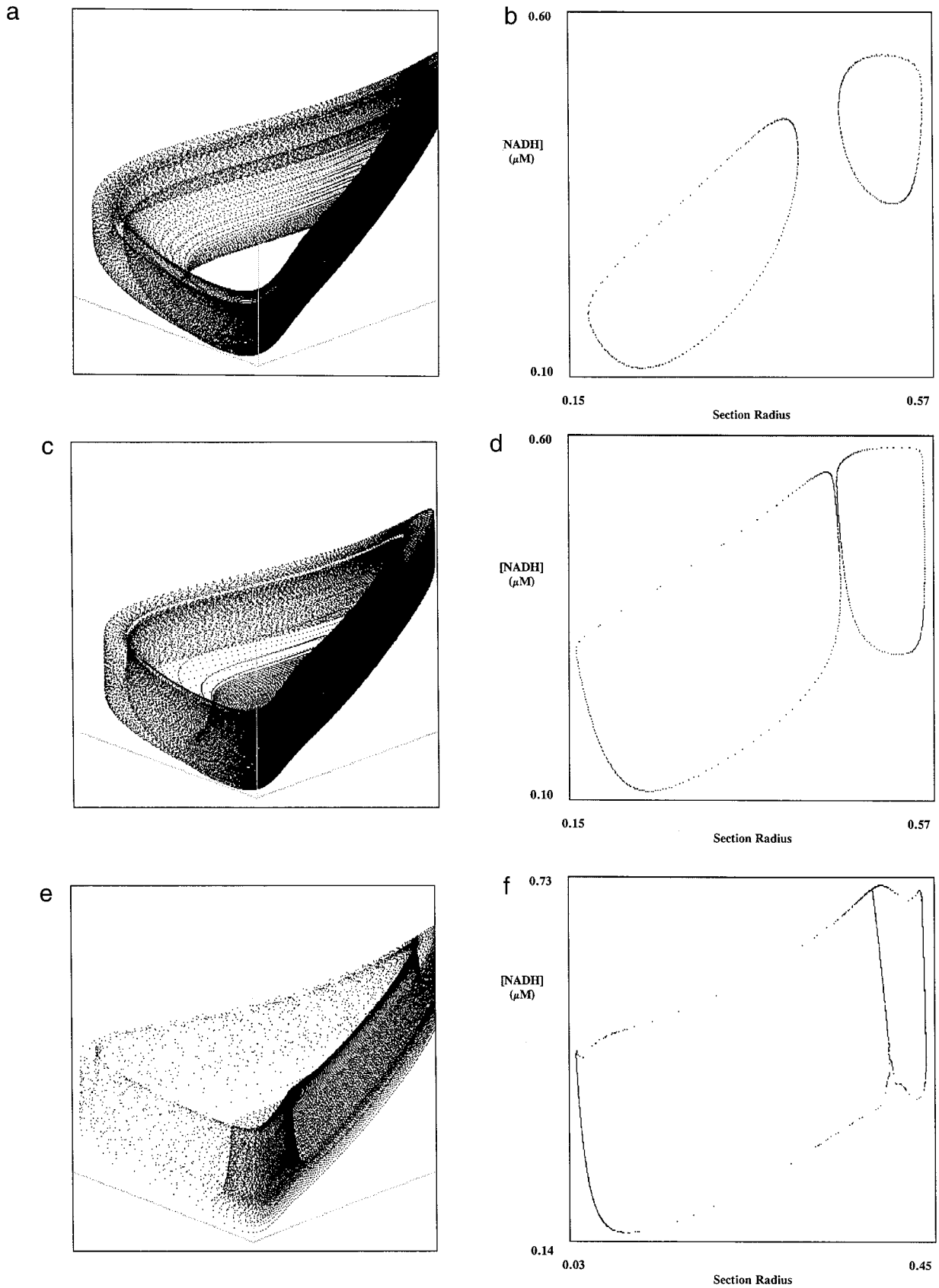

Figure 4. Three-dimensional orbit projections (a, c, e) and Poincaré sections (b, d, f) detailing the evolution of the 1^0-1^1 transitional region. Values of k_9 as in Figure 3b−d, i.e., twice periodic orbit not shown. For the phase portraits, the axes are [O_2], [NAD$^\bullet$], and [NADH]. (a, b) Double torus. NADH input = 0.1226×10^{-6} M s^{-1}. (c, d) Double torus close to tangency. NADH input = 0.1212×10^{-6} M s^{-1}. (e, f) Chaotic flow on a fractal double torus. NADH input = $0.112\,33 \times 10^{-6}$ M s^{-1}.

The transition to chaos occurs just beyond the situation represented by Figure 6d, i.e., at k_9 roughly equal to 1.0×10^{-8} M^{-1} s^{-1}). At this point, we imagine that the unstable manifold of the period-1 saddle cycle crosses over to the other side of the stable manifold. Of course, the two manifolds cannot actually intersect, as this would violate uniqueness. Instead,

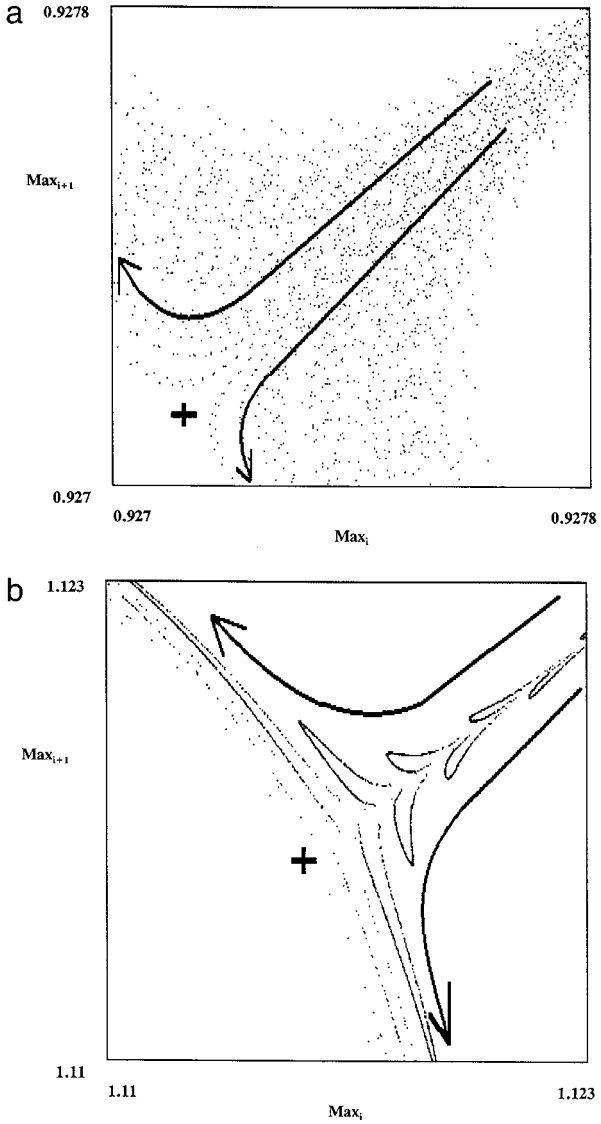

Figure 5. Chaos in the 1^0-1^1 transitional region. Magnified next amplitude maps. Approximate location of the period-1 fixed point is indicated by + signs; direction of itineraries approaching and diverging from the fixed point, by arrows. (a) $k_9 = 0.7 \times 10^8$ M^{-1} s^{-1}; NADH input = $0.112\,33 \times 10^{-6}$ M s^{-1}. (b) $k_9 = 0.6 \times 10^8$ M^{-1} s^{-1}; NADH input = $0.105\,00 \times 10^{-6}$ M s^{-1}.

they wind about each other in an incredibly complex fashion so as to produce a homoclinic tangle. Some of this complexity can be seen in the next amplitude maps shown in Figure 5. Homoclinic tangles are, of course, sure indicators of chaotic sets[21] containing infinite numbers of periodic and aperiodic motions "glued" together by a dense orbit. For a general discussion of homoclinic tori, see Chapter 3 of Wiggens.[22]

The preceding scenario nicely explains the evolution of chaos in the transitional regions between adjacent MMOs. Moreover, FTBs are a possibility in just about every situation that evidences period-doubling, provided the dimension of the motion is greater than 2. For example, as discussed in ref 23, period-doubling in two-dimensional maps, which may be used to model three-dimensional flows, necessarily entails a range of parameter values for which the eigenvalues are complex. This, in turn, sets the stage for secondary quasiperiodicity,[20] i.e., motion on a period-doubled torus, which is the necessary precondition for an FTB. In short, FTBs may occur in a variety of experimental and theoretical contexts.

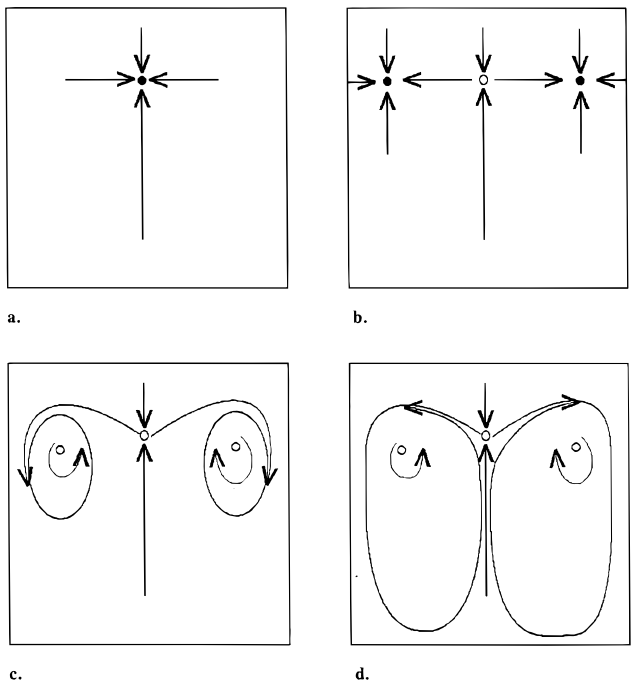

Figure 6. Schematic representation (Poincaré sections) of the approach to homoclinicity in the 1^0-1^1 region in response to decreasing values of k_9. Stable points are represented by filled circles; unstable points, by open circles; and stable and unstable manifolds by lines and arrows. (a) For high values of k_9, the period-1 cycle is stable in both directions. (b) Period-doubling destabilizes the period-1 cycle which now becomes a saddle. (c) The period-2 cycle emits a 2-torus and is itself thereby destabilized. (d) The 2-torus fattens (and approaches coincidence with the unstable manifold of the period-1 cycle) with the consequence that its medial surfaces approach the stable manifold of the period-1 cycle. Since the two manifolds cannot intersect, further reductions in k_9 result in the medial surfaces being braided about each other and the stable manifold of the period-1 cycle.

Homoclinic "explosions" have a number of interesting properties that distinguish them from the more familiar period-doubling route to chaos. The most pertinent of these are as follows: (i) the transition to chaos is instantaneous; (ii) true chaos, as opposed to the necessarily ambiguous dense bands generated by the computer, can exist over open intervals of parameter values. Thus, the situation in BFSO is thus reminiscent of that observed in the Lorenz system,[24] in which case a homoclinic bifurcation gives rise to a chaotic saddle and ultimately the strange attractor.

Higher Order Transitions. A similar evolution (Figures 7−9) is observed in the transitional regions between higher order MMOs. Figures 7 and 8 give details for the 1^1-1^2 transition. Here, we show a bifurcation diagram and quasiperiodic Poincaré section for $k_9 = 0.63 \times 10^8$ M^{-1} s^{-1} (Figure 7) and a chaotic Poincaré section and magnifications thereof in Figure 8. Again, the response to reducing k_9 is

period-doubling → secondary quasiperiodicity → period-doubled fractal tori

Note that the vertical line at the left of the section in Figure 8a is, in fact, a highly compressed copy (Figure 8c) of the piece at the right. This reflects the fact that the transition to chaos involves a quadruple, as opposed to a double, torus. Similar results obtain for the 1^2-1^3 (Figure 9) and 1^3-1^4 regions (not shown).

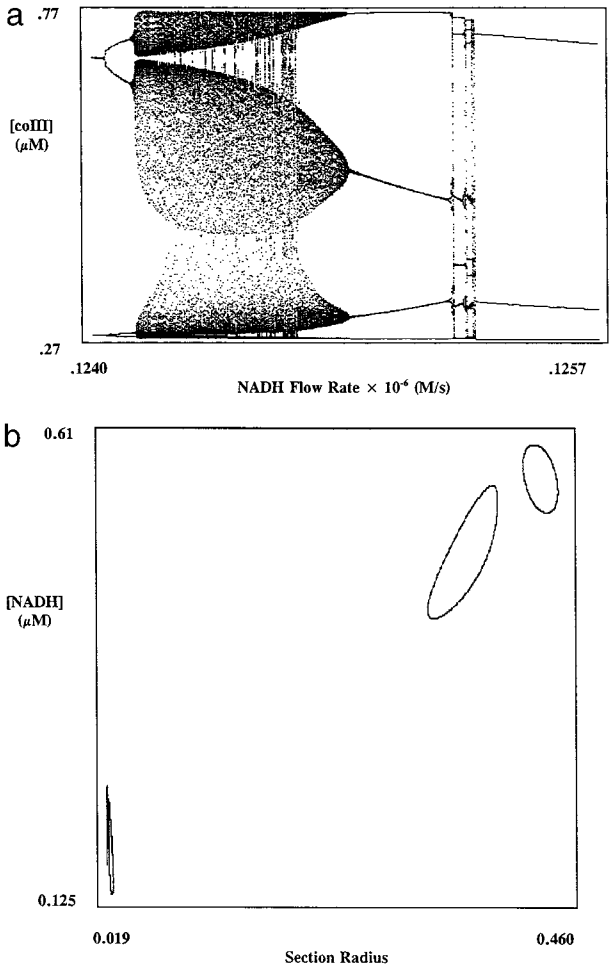

Figure 7. Fat torus route to chaos in the 1^1-1^2 transitional region. $k_9 = 0.63 \times 10^8$ M^{-1} s^{-1}. (a) Bifurcation diagram. (b) Poincaré section evidencing quasiperiodicity. (NADH input = 0.124 14 $\times 10^{-6}$ M s^{-1}).

V. Discussion

Modulo our inability to detect an asymptotic state corresponding to alternating 1^3 and 1^4 cycles in the 1^3-1^4 region, the simulations reported in section III are consistent with the succession of dynamical states observed experimentally. The numerics thus provide considerable support for the BFSO model. Taken together with previous studies,[1,3,4] they suggest that BFSO is remarkably adept at reproducing the experimental essentials, the liberties[1,4] it takes with the known chemistry notwithstanding. Of course, as in all attempts to model the PO reaction published to date, the agreement between theory and observation is only qualitative. Failure of the model to give quantitative agreement with experiment may result from at least four factors:

1. The model is only an approximation of the true mechanism. For example, the modifiers methylene blue (MB) and 2,4-dichlorophenol (DCP) do not enter as explicit variables, their concentrations being instead reflected by values of the rate constants.

2. Many of the rate constants are but order of magnitude approximations.

3. The average concentration of NADH in solution, $[NADH]_{av}$, is not uniquely determined by the rate of NADH input, and its use as an experimental bifurcation parameter can therefore lead to errors in interpretation, for example, in the case that the bifurcation diagram has multiple branches.

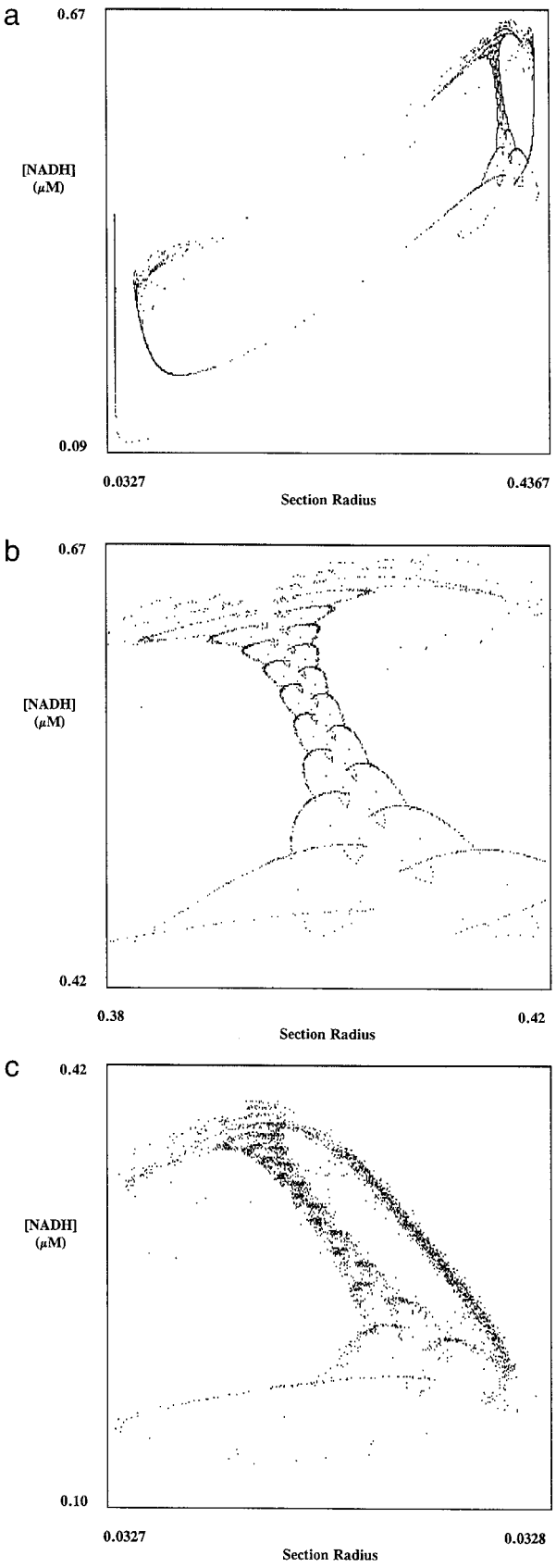

Figure 8. Chaos on a fractal quadruple torus in the 1^1-1^2 transition region. $k_9 = 0.48 \times 10^8$ M^{-1} s^{-1}; NADH input = 0.1181 $\times 10^{-6}$ M s^{-1}. (a) Poincaré section. (b) Magnification of the tangled region at the right side of the section. (c) Magnification of the vertical line at the left of the section reveals a compressed copy of the right side of the section.

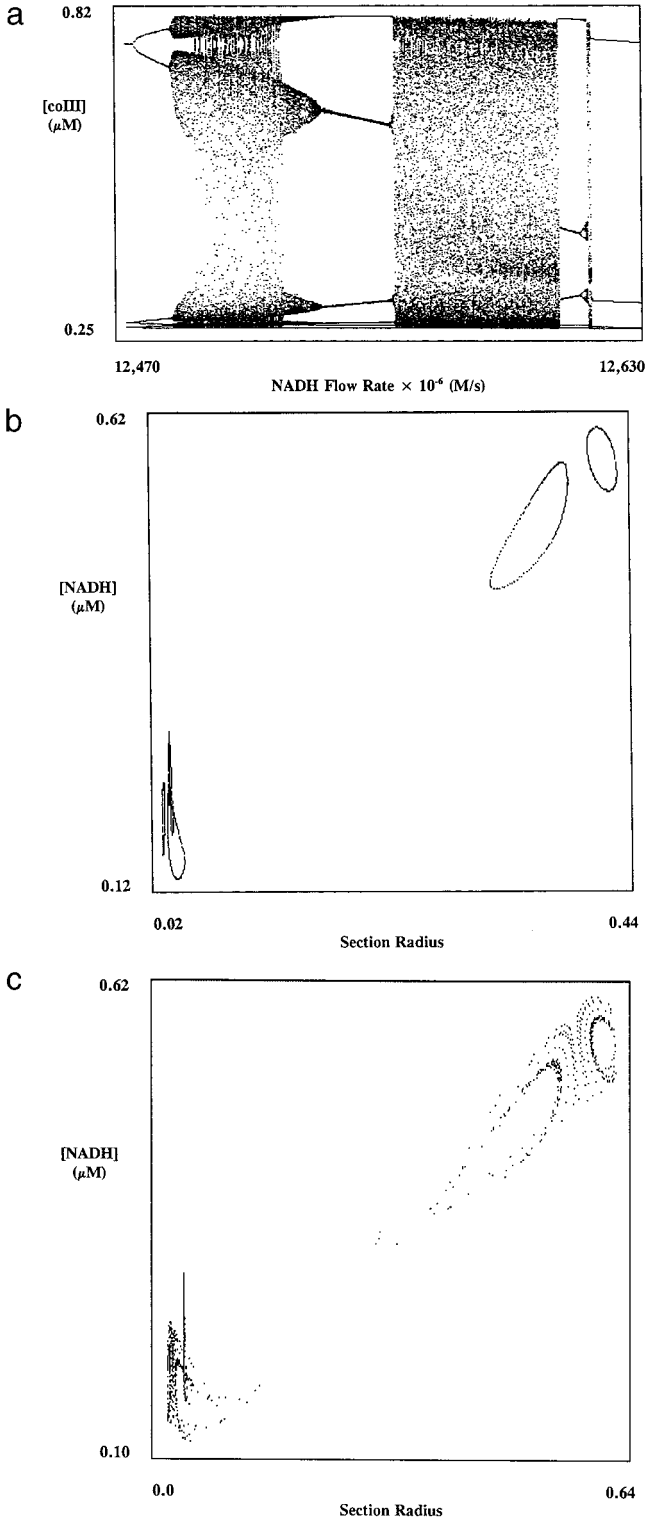

Figure 9. The 1^2-1^3 transition regions. $k_9 = 0.502 \times 10^8$ M^{-1} s^{-1}. (a) Bifurcation diagram. (b) Quasiperiodic Poincaré section. NADH input = $0.124\,85 \times 10^{-6}$ M s^{-1}. (c) Chaotic Poincaré section. NADH input = $0.124\,95 \times 10^{-6}$ M s^{-1}.

4. The decision to model changing pH values by varying a single rate constant is undoubtedly an oversimplification. More plausibly, the values of several such constants are pH-dependent.

With regard to the final point and, as shall be discussed in a forthcoming publication, we note that these discrepancies are diminished if a more realistic approach to pH is undertaken. In this case, i.e., if several rate constants are adjusted simultaneously, improved quantitative agreement between model and experiment results.

Our results also make for additional testable predictions. Principal among these are the following:

1. The existence of dynamical states, such as chaos in the 1^0-1^1 region, which have not yet been observed experimentally.

2. The association of transitional chaos with period-doubled fractal tori.

We emphasize that the second prediction may be chemically important. Specifically, we note that although many chemical models[13,14,16,25−35] predict period-adding or Farey-ordered sequences of MMOs along with intervening regions of complex dynamics, there appears to be **no necessary association** between transitional chaos and the fat torus scenario. For example, exploratory investigations of both the abstract oscillatory scheme proposed by Petrov et al.[32] and the Olsen[36] model of the PO reaction at once yield ample evidence of transitional chaos but no suggestion of period-doubled tori, fractal or otherwise. The fat torus scenario may thus prove to be a qualitative criterion by which alternative models of the PO reaction may be distinguished. The attractiveness of this possibility should not be underestimated since there now exist a great many models of (1) corresponding to mechanisms that differ in relatively few respects. The possibility that the fat torus scenario may prove useful as a device for culling the crowd of competing models suggests that FTBs in the context of PO chemistry are more than mere mathematical esoterica.

As noted above, the present study points to the potential importance of quasiperiodicity to the evolution of PO dynamics. Because of the extended time series necessary to resolve quasiperiodic states, it is hardly surprising that the experimental evidence for quasiperiodicity in the PO reaction is limited. In fact, there are at present but two observations.[37,33] Of these, one reports that the quasiperiodic state is preceded by large amplitude cycles and followed by small amplitude oscillations, both of which are period-1,[33] while the other merely notes its existence.[37] Of course, the quasiperiodic motions observed experimentally correspond to motion on simple tori—what the authors of ref 20 have termed "primary" quasiperiodicity—and it is intriguing, in this regard, that the reported examples[20] of primary quasiperiodicity in BFSO are associated not with transitions to chaos but, as in ref 33, with shifts from large- to small-amplitude period-1 cycles. By way of contrast, the quasiperiodic transition to chaos described here involves the fractalization of period-doubled tori ("secondary" quasiperiodicity), which, perhaps for the reasons noted above, has not yet been observed in the laboratory.

Finally, the results reported here have some very general implications for peroxidase-oxidase dynamics. The first of these relates to the dimension of the motion. Specifically, we observe that *all* of the theoretical discussions of the reaction's dynamics implicitly assume motion that is effectively three-dimensional. But BFSO has 10 independent variables. In other words, the dimension of the ambient vector space is also 10, leaving one to wonder as to whether it even makes sense to analyze three-dimensional projections or, in the case of experimental data, three-dimensional reconstructions. The observation of FTBs in BFSO strongly suggests that the dynamics are, in fact, played out in a three-dimensional subspace of R^{10}. This is because FTBs involving two-tori (T^2) are not generic in higher dimensions. In spaces of dimension 4 and greater, the pieces of torus will, with probability 1, push past each other without the occurrence of a homoclinic event. In short, the observation of FTBs in BFSO suggests that a three-dimensional approach to

PO dynamics is justified. This conclusion marches well with other theoretical studies[12,38] in which simpler models (three or four equations) have been derived from more complex schemes such as BFSO via separation of time-scale arguments.

A second implication of the present study (along with as yet unpublished investigations by the senior authors) is that it confirms in a general way the point of view.[12,14,35,39] which holds that the key to understanding the PO reaction is in terms of small-amplitude, high-frequency, quasi-sinusoidal oscillations produced supercritically at one side of the control diagram and large-amplitude, low-frequency, relaxation type oscillations that arise abruptly at the other side. Relative to this perspective, we observe that the chaotic oscillations induced by BFSO in the course of the low- and high-pH simulations are qualitatively distinct. The former derive from the leftward moving bifurcations which start at the right (high NADH) and are of the sort associated with one-dimensional maps, while the latter descend from the fractal tori produced by FTBs and are fundamentally two-dimensional.

Acknowledgment. T.V.B. and W.M.S. thank Aaron King, Mark Kot, and Jay Taylor for discussion. M.J.B.H. and L.F.O. acknowledge financial support by the Danish Natural Science Research Council, the Carlsberg Foundation, and the Novo Nordisk Foundation.

References and Notes

(1) Hauser, M. J. B.; Olsen, L. F.; Bronnikova, T. V.; Schaffer, W. M. *J. Phys. Chem. B* **1997**, *101*, 5075−5083.
(2) Hauser, M. J. B.; Andersen, S.; Olsen, L. F. In *Plant Peroxidases: Biochemistry and Physiology*; Obinger, C., Burner, U., Ebermann, R., Penel, C., Greppin, H., Eds.; University of Geneva, Geneva, 1996; pp 88−93.
(3) Hauser, M. J. B.; Olsen, L. F. *J. Chem. Soc., Faraday Trans.* **1996**, *92*, 2857−2863.
(4) Bronnikova, T. V.; Fed'kina, V. R.; Schaffer, W. M.; Olsen, L. F. *J. Phys. Chem.* **1995**, *99*, 9309−9312.
(5) Olson, D. L.; Williksen, E. P.; Scheeline, A. *J. Am. Chem. Soc.* **1995**, *117*, 2−15.
(6) Fed'kina, V. R.; Ataullakhanov, F. I.; Bronnikova, T. V.; Balabaev, N. K. *Studia Biophys.* **1978**, *72*, 195−202.
(7) Fed'kina, V. R.; Ataullakhanov, F. I.; Bronnikova, T. V. *Biophys. Chem.* **1984**, *19*, 259−264.
(8) Boutelet, I.; Alexandre, S.; Vincent, J.-C. *Eur. J. Biochem.* **1994**, *223*, 489−496.
(9) Fed'kina, V. R.; Bronnikova, T. V. In *Summaries of Reports to All-Union Meeting on Self-Organization in Physical, Chemical and Biological Systems, Sinergetics-86*; Shtinintsa, Kishinev, 1986; p 126.
(10) Fed'kina, V. R.; Ataullakhanov, F. I.; Bronnikova, T. V. *Theor. Exp. Chem.* **1988**, *24*, 165−172.
(11) Aguda, B. D.; Larter, R. *J. Phys. Chem.* **1991**, *95*, 7913−7916.
(12) Fed'kina, V. R.; Bronnikova, T. V.; Ataullakhanov, F. I. *Biofizika* **1992**, *37*, 885−894.
(13) Larter, R.; Olsen, L. F.; Steinmetz, C. G.; Geest, T. In *Chaos in Chemistry and Biology*; Field, R. J., Györgyi, L., Eds.; World Scientific: Singapore, 1993; pp 175−224.
(14) Fed'kina, V. R.; Bronnikova, T. V. *Biofizika* **1995**, *40*, 36−47.
(15) Hung, Y.-F.; Schreiber, I.; Ross, J. *J. Phys. Chem.* **1995**, *99*, 1980−1987.
(16) Larter, R.; Hemkin, S. *J. Phys. Chem.* **1996**, *100*, 18924−18930.
(17) Schreiber, I.; Hung, Y.-F.; Ross, J. *J. Phys. Chem.* **1996**, *100*, 8556−8566.
(18) Yokota, K.; Yamazaki, I. *Biochemistry* **1977**, *16*, 1913−1920.
(19) Knobloch, E.; Weiss, N. O. *Phys. Lett.* **1981**, *85A*, 127−130.
(20) Bronnikova, T. V.; Schaffer, W. M.; Olsen, L. F. *J. Chem. Phys.* **1996**, *105*, 10849−10859.
(21) Guckenheimer, J.; Holmes, P. *Nonlinear Oscillations, Dynamical Systems and Bifurcations of Vector Fields*; Springer-Verlag: New York, 1983.
(22) Wiggens, S. *Global Bifurcations and Chaos*; Springer-Verlag: New York, 1988.
(23) Aronson, D. G.; Chory, M. A.; Hall, A.; McGehee, R. P. *Commun. Math. Phys.* **1981**, *83*, 303−351.
(24) Sparrow, C. *The Lorenz Equations: Bifurcations, Chaos and Strange Attractors*; Springer-Verlag: New York, 1982.
(25) Larter, R.; Bush, C. L.; Lonis, T. R.; Aguda, B. D. *J. Chem. Phys.* **1987**, *87*, 5765−5771.
(26) Barkley, D. *Phys. Lett. A* **1988**, *129*, 219−222.
(27) Aguda, B. D.; Larter, R.; Clark, B. L. *J. Chem. Phys.* **1989**, *90*, 4168−4175.
(28) Steinmetz, C. G.; Larter, R. *J. Chem. Phys.* **1991**, *94*, 1388−1396.
(29) Györgyi, L.; Field, R. J. *J. Chem. Phys.* **1991**, *95*, 6594−6602.
(30) Györgyi, L.; Field, R. J. *Nature* **1992**, *355*, 808−810.
(31) Györgyi, L.; Field, R. J.; Noszticzius, Z.; McCormick, W. D.; Swinney, H. L. *J. Chem. Phys.* **1992**, *96*, 1228−1233.
(32) Petrov, V.; Scott, S. K.; Showalter, K. *J. Chem. Phys.* **1992**, *97*, 6191−6198.
(33) Hauck, T.; Schneider, F. W. *J. Phys. Chem.* **1993**, *97*, 391−397.
(34) Hauck, T.; Schneider, F. W. *J. Phys. Chem.* **1994**, *98*, 2072−2077.
(35) Fed'kina, V. R.; Bronnikova, T. V.; Olsen, L. F.; Schaffer, W. M., manuscript in preparation.
(36) Olsen, L. F. *Phys. Lett. A* **1983**, *94*, 454−457.
(37) Samples, M. S.; Hung, Y.-F.; Ross, J. *J. Phys. Chem.* **1992**, *96*, 7338−7343.
(38) Bensen, D. S.; Scheeline, A. *J. Phys. Chem.* **1996**, *100*, 18911−18915.
(39) Fed'kina, V. R.; Bronnikova, T. V. *Biofizika* **1994**, *39*, 599−607.